

## Catalytic Membrane Reactor: Multilayer membranes elaboration

A. Julian<sup>1,2,\*</sup>, E. Juste<sup>1,2</sup>, T. Chartier<sup>1</sup>, P. Del Gallo<sup>2</sup>, N. Richet<sup>2</sup>

<sup>1</sup>SPCTS, CNRS, ENSCI, 47 avenue Albert Thomas, 87065 Limoges, France

<sup>2</sup>Air Liquide, Centre de Recherche Claude-Delorme, 1 chemin de la porte des Loges, 78354 Jouy-en-Josas Cedex, France

### Abstract

Methane conversion to syngas is very attractive for hydrogen or clean fuel production and provides an alternative to oil products.

An efficient architecture for the membrane reactor is constituted of a porous support, a thin dense membrane and a catalyst layer.

This work is focused on the elaboration process of such asymmetric membranes by co-sintering of at least the porous support and the dense membrane and specially the choice of well adapted materials.

$\text{La}_{0.8}\text{Sr}_{0.2}\text{Fe}_{0.7}\text{Ga}_{0.3}\text{O}_{3-\delta}$  perovskite material has been chosen as the dense membrane because it exhibits a good compromise between oxygen flux and stability.

The choice of the material for the porous support is mainly oriented by the sintering behaviour of the membrane, the thermal expansion behaviour of both layers to avoid cracks formation under working conditions and the chemical inertness of both materials. Several formulations fulfilling these three requirements were synthesized by liquid phase reaction and tape-cast. A pore forming agent was added in the support tape-casting slurry in order to create a controlled porosity. Then, the porous support has been characterized in term of gas permeability and thermal expansion under working conditions.

**Keywords:** Ceramic membrane, co-sintering, perovskite, syngas, mixed conducting materials.

### Introduction

Membrane reactors with mixed oxygen-ionic and electronic conductivities are of great interest for natural gas conversion into value-added products such as syngas ( $\text{CO}+\text{H}_2$ ).

Perovskite-type oxides ( $\text{ABO}_3$ ) suitably doped on the A and/or B site exhibit both ionic and electronic conductivity at temperatures typically higher than  $700^\circ\text{C}$ . [1-4] These materials allow oxygen diffusion between the opposite faces of the reactor thanks to a differential pressure driven mode without the need of external electrodes.

Membranes have to satisfy many requirements such as high oxygen permeation rates, long-term chemical and thermal stability under working conditions and good mechanical properties [5-7]. In order to improve both mechanical properties and oxygen permeation rate, it has been proposed to separate the two functions by using a porous substrate coated by a thin membrane

layer. The porous layer ensures mechanical properties and access of air to dense membrane which ensures oxygen diffusion. A catalytic layer should be added to catalyze methane reforming (Figure 1). This paper focuses on the study of  $\text{La}_{0.8}\text{Sr}_{0.2}\text{Fe}_{0.7}\text{Ga}_{0.3}\text{O}_{3-\delta}$  as dense membrane.

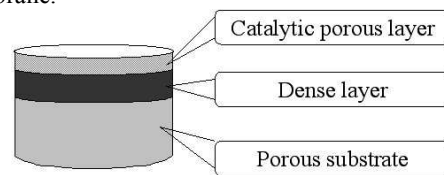


Figure 1: Schematic view of a multilayer membrane.

A challenging problem is to find a material for the porous layer. This material must satisfy some requirements such as chemical compatibility with dense membrane, same conditions of sintering with similar shrinkage behaviour, similar thermal expansion.

A first solution consists in using the same material for the dense and the porous membranes, but raw-materials of gallium are very expensive and the cost of catalytic membrane reactor has to be decreased for an industrial use.

This paper proposes to study a second solution with  $\text{La}_{0.8}\text{Sr}_{0.2}\text{FeO}_{3-\delta}$  as support material.

### Experimental

#### Powder synthesis

$\text{La}_{0.8}\text{Sr}_{0.2}\text{FeO}_{3-\delta}$  powder (referenced as LSF 821) was synthesized by a citrate route [8]. Metal precursors  $\text{La}(\text{NO}_3)_3 \cdot 6\text{H}_2\text{O}$ ,  $\text{Sr}(\text{NO}_3)_2$ ,  $\text{Fe}(\text{NO}_3)_3 \cdot 9\text{H}_2\text{O}$  (Alfa Aesar) were mixed in aqueous solution in the stoichiometric amount. Citric acid is added with a molar ratio [citric acid]/[metal ions] of 1.5. Then pH is adjusted by adding an ammoniac solution. After evaporation of solvent, an amorphous precursor is obtained by heating at  $200\text{--}250^\circ\text{C}$ . The powder is obtained by calcination at  $1000^\circ\text{C}$  during 12h. The synthesized powder is attrition milled in ethanol to reach a mean grain size of  $0.45\mu\text{m}$ .

Dense membrane material  $\text{La}_{0.8}\text{Sr}_{0.2}\text{Fe}_{0.7}\text{Ga}_{0.3}\text{O}_{3-\delta}$  (referenced as LSFG 8273) is supplied by Pharmacie Centrale de France. Grain size of  $0.3\mu\text{m}$  is obtained by attrition-milling.

#### Multilayers elaboration

Dense membrane and porous substrate are tape-cast [9]. Powders were planetary milled for 4h in azeotropic mixture of butanone-2 and ethanol with a dispersant. Then, an acrylic binder (methyl methacrylate, Degalan

LP51/07 Degussa) and a phthalate plasticizer (dibutyl phthalate, Sigma-Aldrich) were added to the slurry with a subsequent ball-milling of 12h. Porous membranes were obtained by adding corn starch, as pore forming agent, in the slurry after 12h ball-milling stage and with a subsequent 4hrs ball-milling.

The suspensions were de-aired for 48h at a very slow rotation speed and tape-cast to obtain 150 $\mu$ m green tapes. Then, 30-mm disks were punched from the tapes, stacked and laminated under a pressure of 50MPa at a temperature of 85°C. Asymmetric membranes were obtained by stacking 7 disks of a corn starch containing tape (LSF 821) and one disk of a tape without pore-forming agent (LSFG 8273).

All membranes were slowly debinded at 650°C in air and sintered at 1250°C for 2h in air.

### Characterizations

Phase crystallographic structures are determined by XRD using a Debye Scherrer system. Specific surface area is controlled by BET method (Micromeritics, ASAP-2010) and grain size by a laser granulometer during attrition milling (Malvern Instruments, Mastersizer 2000). The density of sintered samples is measured by the Archimedes' method and microstructure is observed on polished cross sections by SEM (S-2500, Hitachi). Sintering shrinkage and thermal expansion in air are measured by dilatometry (Setsoft, SETARAM).

Gas permeability is measured using a nitrogen flow (Figure 2). Porous membranes are sealed on an alumina tube with a polymeric adhesive and are submitted to nitrogen pressure flow on one side while the other side is at atmospheric pressure. Pressure drop between the two faces is measured by a pressure sensor and the nitrogen flow is controlled with a flowmeter.

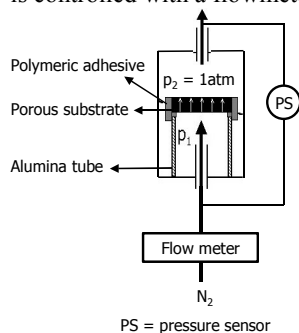


Figure 2 : Schematic view of the permeability measurement device.

## Results and discussion

### Structural analysis

Densities of powders measured with a helium pycnometer are reported on Table 1.

Composition	Density kg/m <sup>3</sup>	Specific area m <sup>2</sup> /g
LSFG 8273	6.40	10.04
LSF 821	6.34	7.30

Table 1: Powders characteristics.

Powders show perovskite-type structure and no secondary phases are detected in the limit threshold (Figure 3).

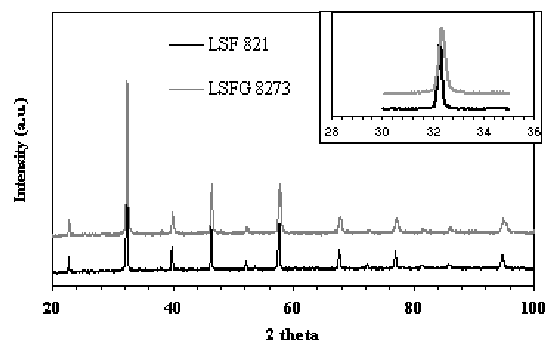


Figure 3: XRD of LSF 821 and LSFG 8273.

Lattice parameters are refined using the full-profile Rietveld method using silicium as an internal standard (Tab.2). Orthorhombic structure (Pbnm space group) is found for LSF 821 and LSFG 8273 was refined with a monoclinic structure (P 2/C space group) [10-11].

Composition	a Å	b Å	c Å	$\alpha$ °
La <sub>0.8</sub> Sr <sub>0.2</sub> Fe <sub>0.7</sub> Ga <sub>0.3</sub> O <sub>3-<math>\delta</math></sub>	7.816 <sub>9</sub>	5.547 <sub>1</sub>	5.526 <sub>7</sub>	90.1
La <sub>0.8</sub> Sr <sub>0.2</sub> FeO <sub>3-<math>\delta</math></sub>	5,527 <sub>8</sub>	5,553 <sub>2</sub>	7,818 <sub>0</sub>	90

Table 2: Lattice parameters of LSF821 and LSFG8273.

### Co-sintering

Porous LSF 821 and dense LSFG 8273 have been co-fired to obtain a plane asymmetric membrane.

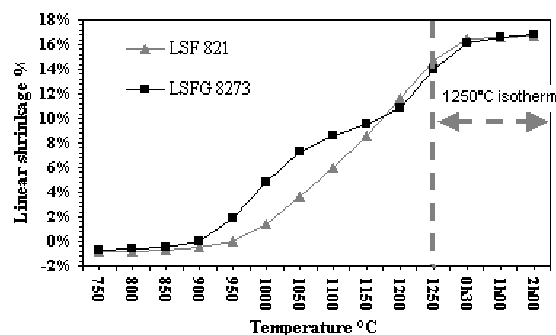


Figure 4: Linear shrinkage of LSF 821 and LSFG 8273 during sintering in air.

Flat crack free asymmetric LSF 821/LSFG 8273 membranes can be obtained by sintering at 1250°C during 2h, because of similar final shrinkages and sintering behaviours.

Perovskite materials present particular thermal expansion behaviour. Thermal Expansion Coefficient (TEC) increases at high temperature ( $T > T^*$ ) (Figure 5) because of oxygen departure. Oxygen vacancies are created above a temperature threshold, in equilibrium with the oxygen partial pressure, that causes coulomb repulsion of cations and the reduction of Fe<sup>4+</sup> to Fe<sup>3+</sup> and then increase of the cell volume [3, 4, 6, 7].

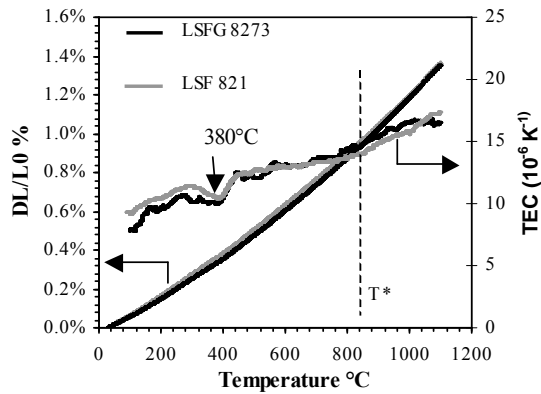


Figure 5: Linear dilatation and TEC of LSF 821 and LSGF 8273 in function of temperature in air.

The average TEC of the two materials are very close, both at low and high temperatures (Table 3). The discontinuity on first derivative curve at about 380°C is due to the monoclinic (or orthorhombic) to rhombohedra phase transition. This phase transition occurs at the same temperature for the two materials. TEC values for low temperature are considered between 400°C and 800°C.

Composition	Average TEC ( $10^{-6} \text{ K}^{-1}$ ) in air	
	$\alpha_{T < T^*}$	$\alpha_{T > T^*}$
$\text{La}_{0.8}\text{Sr}_{0.2}\text{Fe}_{0.7}\text{Ga}_{0.3}\text{O}_{3-\delta}$	12.02	16.25
$\text{La}_{0.8}\text{Sr}_{0.2}\text{FeO}_{3-\delta}$	12.40	15.82

Table 3: Average TEC of LSF 821 and LSGF 8273.

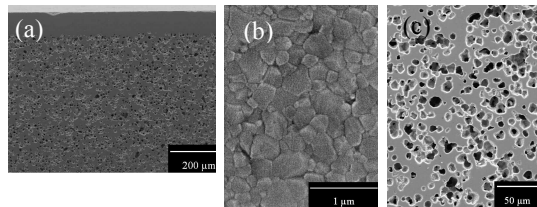


Figure 6: SEM observations of (a) dense/porous interface, (b) dense membrane and (c) porous substrate.

After sintering at 1250°C-2h, LSGF 8273 membrane is densified at more than 98% of theoretical density. Porosity of porous substrate is totally open and is around 34%. No delamination or cracks are observed on the dense/porous interface.

### Permeability

Porous substrate must not slow down the air flow that reaches the dense membrane. Several amounts of pore forming agent have been introduced in the tape-casting slurry to lead to final porosity values ranging from 26% to 41%.

Pores are organized in a more or less complex network [12-13]. Three kinds of pores can be defined (Figure 7):

- Interconnected pores: pores form a continuous path through the support layer,
- Ox-bow: Pores that are connected only on one side,
- Closed pores.

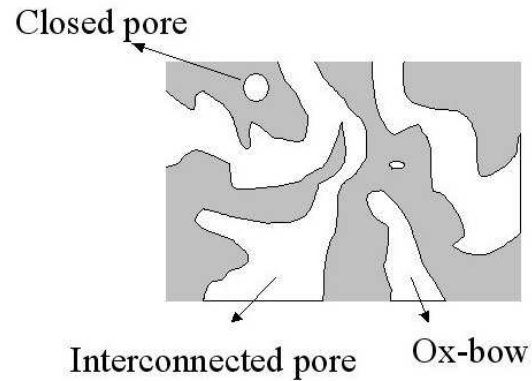


Figure 7: Typical porous structure.

The open porosity, measured by the Archimedes' method, gathers the two first kinds of pores. Porous volume is characterized by its tortuosity and connectivity. Tortuosity is defined as the ratio of the real distance covered by molecules  $L$  on the Euclidean distance  $L_e$ .

$$\tau = \frac{L}{L_e} \quad (1)$$

Three kinds of flows can be considered: (i) the Knudsen diffusion for small pores, (ii) slip flow and (iii) viscous flow for larger pores. The flow regime is determined by the Knudsen number  $K=D/\lambda$  where  $D$  is the pore diameter and  $\lambda$  is the mean free path of the gas (65nm for nitrogen). When the diameter of pores is lower than the mean free path of the gas molecules, the Knudsen number is lower than unity and so Knudsen flow is dominant. For larger pore size, where the ratio is higher than 10, Poiseuille flow dominates with a contribution of slip flow. In our case, Knudsen number is very high and so Knudsen diffusion can be neglected and viscous flow is dominant [14].

In the case of incompressible gas and laminar flow, Darcy law can be used:

$$\frac{Q}{S} = \frac{k_a}{2 \cdot \mu \cdot L \cdot P} (P_1^2 - P_2^2) = \frac{k_a}{2 \cdot \mu \cdot L \cdot P} P_m \cdot \Delta P \quad (2)$$

with  $Q$  the flow of nitrogen ( $\text{m}^3 \cdot \text{s}^{-1}$ ),  $S$  ( $\text{m}^2$ ) the membrane area,  $k_a$  ( $\text{m}^2$ ) the apparent permeability,  $\mu$  (Pa.s) the gas viscosity,  $L$  (m) the membrane thickness,  $P_m$  (Pa) the average pressure ( $(p_1+p_2)/2$ ) and  $\Delta P$  (Pa) the pressure drop ( $p_1-p_2$ ). Only an apparent permeability can be calculated since the flow is not exclusively viscous.

The Reynolds number makes it possible to determine if the flow is laminar or turbulent:

$$\text{Re} = \frac{d_h \cdot \rho \cdot v}{\mu} \quad (3)$$

$d_h$ ,  $\rho$  and  $v$ , are respectively the hydraulic diameter of pores (m), the density ( $\text{kg} \cdot \text{m}^{-3}$ ) and the velocity ( $\text{m} \cdot \text{s}^{-1}$ ). For laminar flows through a membrane, Carman and Klinkenberg have proposed to express volumetric flow rate  $Q$  as a function of the average pressure:

$$\frac{Q}{S \cdot \Delta P} = A \cdot P_m + B \quad (4)$$

with  $A$  a constant representing viscous flow  $B$  a constant corresponding to non viscous flow.

$$A = \frac{k_v}{R.T.\mu.L} \quad (5)$$

where  $k_v = (\varepsilon/8.\tau)r_p^2$  (m<sup>2</sup>) is the intrinsic permeability corresponding to viscous flow,  $\varepsilon$  the porosity;  $\tau$  the tortuosity,  $r_p$  (m) the pore radius,  $R$  the gas constant and  $T$  (K) the temperature.

$$B = \frac{4.\bar{V}}{3.R.T.L} k_{nv} \quad (6)$$

where  $k_{nv} = (\varepsilon/2.\tau)r_p$  (m) is the intrinsic permeability corresponding to slip flow,  $\bar{V} = \sqrt{8RT/\pi M}$  is the mean molecular velocity.  $M$  is the molecular mass of the gas molecule.

The intrinsic permeabilities  $k_v$  and  $k_{nv}$  respectively for viscous flow and for slip flow can be calculated from gas permeability measurements.

From Eq. (4), (5) and (6), pore radius and tortuosity can be calculated:

$$r_p = \frac{16.A.\mu}{3.B} \sqrt{\frac{8RT}{\pi M}} \quad (7)$$

$$\tau = \frac{256.\varepsilon.A}{9.B^2.\pi.M.L} \mu \quad (8)$$

Eq. (4), (5), (6), (7) and (8) are written using the approximation of capillary tubes. The pore radius and tortuosity calculated are then approximations.

Permeability of the porous substrate is measured using the device represented in Figure 2. Samples are ceramic disks of 24mm diameter and 1mm thick with different porosity values ranging from 26% to 41%. In our range of pore size, the Reynolds (Eq. 3) number is less than  $1 \times 10^{-2}$  and thus laminar flow can be considered.

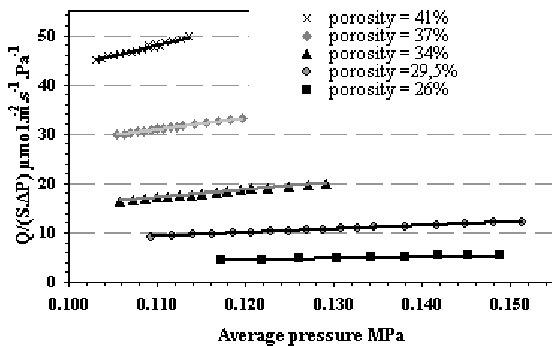


Figure 8: Evolution of nitrogen flow in function of porosity.

Nitrogen flow through porous support increases with porosity (Figure 8).

Pore radius ( $\mu\text{m}$ ) and tortuosity have been calculated (Figure 9).

When the amount of pore agent forming in the suspension increases, first tortuosity decreases, and the pore radius slowly increases and nitrogen flow raises. Pores, initially only connected on one side become

interconnected pores. Then, when porosity exceeds a critical value (about 33%), tortuosity increases probably due to the increase of the number of possible paths for gas and the pore radius also increases.

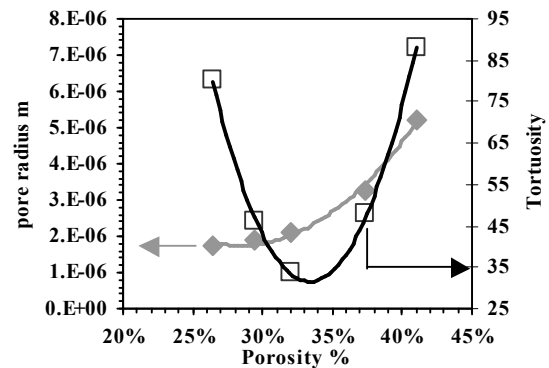


Figure 9: Pore radius (m) and tortuosity in function of porosity.

Contact area with gas will be increased with porosity which can be profitable for oxygen permeation through the dense membrane because the porous support is active for oxygen permeation. However, the porosity of the support is detrimental for good mechanical properties.

Asymmetric membranes with supports of different porosity characteristics (volume, size, tortuosity) have to be tested in term of oxygen permeation in order to know the influence of the area of contact between the porous support and gas phase on the membrane performances.

## Conclusions

A plane asymmetric membrane was obtained by tape-casting and co-sintering of dense LSF823 membrane and porous LSF821 support. Sintering behaviour and thermal expansion of these two materials have been adapted and are very similar at high temperature under air. No cracks and no delamination have been observed on a cross section of asymmetric membrane. Influence of the concentration of pore forming agent on permeability and tortuosity have been studied. A compromise between air flow, which requires a high porosity, and mechanical properties will have to be found. The influence of the porosity characteristics (volume, size, tortuosity) on the membrane performances remains to be studied.

## References

1. Y. Teraoka and all, Mixed ionic-electronic conductivity of  $\text{La}_{1-x}\text{Sr}_x\text{Co}_{1-y}\text{Fe}_y\text{O}_{3-\delta}$  perovskite-type oxides, Mater. Res. Bull. **23** (1988) 51-58.
2. Y. Teraoka and all, Oxygen permeation through perovskite-type oxides, Chemical letter (1985), 1743-1746.

3. V. V. Kharton and all, Perovskite-type oxides for high temperature oxygen separation membranes, *Journal of Membrane Science* **163** (1999), 307-317
4. H. J. M. Bouwmeester, Dense ceramic membranes for methane conversion, *Catalysis Today* **82** (2003), 141-150.
5. S. Kim and all, Oxygen surface exchange in mixed ionic electronic conductors: application to  $\text{La}_{0.5}\text{Sr}_{0.5}\text{Fe}_{0.8}\text{Ga}_{0.2}\text{O}_{3-\delta}$ . *Journal Electrochemistry Society* **147** (2000), 2398-2406.
6. V. V. Kharton and all, Perovskite-like system (Sr, La)(Fe, Ga) $\text{O}_{3-\delta}$  : structure and ionic transport under oxidizing conditions. *Solid State ionics* **150** (2002), 229-243.
7. V.V. Kharton and all, Thermal and chemical induced expansion of  $\text{La}_{0.8}\text{Sr}_{0.2}(\text{Fe, Ga})\text{O}_{3-\delta}$  ceramics, *Journal of the European Ceramic Society* **23** (2003), 1417-1426.
8. Q. Xu and all, Citrate method synthesis, characterization and mixed electronic-ionic conduction properties of  $\text{La}_{0.6}\text{Sr}_{0.4}\text{Co}_{0.8}\text{Fe}_{0.2}\text{O}_{3-\delta}$  perovskite-type complex oxides, *Scripta Materialia* **50** (2004), 165-170.
9. G. Etchegoyen and all, Microstructure and oxygen permeability of  $\text{La}_{0.6}\text{Sr}_{0.4}\text{Fe}_{0.9}\text{Ga}_{0.1}\text{O}_{3-\delta}$  membrane containing magnesia as dispersed second phase particles, *Journal of Membrane science* **286** (2006), 86-95
10. P.Ciambelli and all, La, Ca and Fe oxide perovskites : preparation, characterization and catalytic properties for methane combustion, *Applied Catalysis B : Environmental* **33** (2001), 193-203
11. M.V. Patrakeev and all, Electron/hole and ion transport in  $\text{La}_{1-x}\text{Sr}_x\text{FeO}_{3-\delta}$ , *Journal of solid state chemistry* **172** (2003), 219-231
12. V. Picandet, Influence d'un endommagement a mécanique sur la perméabilité et sur la diffusivité hydrique des bétons, Thesis (2001)
13. A. Laghcha, Contribution a l'étude des transferts gazeux et liquide au sein des parois en béton endommagées sous sollicitation thermo-hydrique, thesis 2006
14. J WOO Yun and all, Permeability of green ceramic tapes as a function of binder loading, *Journal of the American Ceramic Society* **90** (2007), 456-461.